Pharm Res (2014) 31:847–860
DOI 10.1007/s11095-013-1207-0

RESEARCH PAPER

Breast Cancer Resistance Protein-Mediated Efflux of Luteolin Glucuronides in HeLa Cells Overexpressing UDP-Glucuronosyltransferase 1A9

Lan Tang • Ye Li • Wei-Ying Chen • Shan Zeng • Ling-Na Dong • Xiao-Juan Peng • Wen Jiang • Ming Hu • Zhong-Qiu Liu

Received: 4 February 2013 / Accepted: 12 September 2013 / Published online: 3 October 2013

ABSTRACT

Purpose UDP-glucuronosyltransferases (UGTs) are responsible for the formation of glucuronides of polyphenolic flavonoids. This study investigated the UGT1A9-mediated glucuronidation of luteolin and the kinetics of luteolin glucuronide efflux.

Method HeLa cells overexpressing UGT1A9 (HeLa-UGT1A9) were used to determine the kinetics of breast cancer resistance protein (BCRP)-mediated transport of luteolin glucuronides. Human UGT isoforms were used to determine glucuronidation rates.

Results UGT1A9 was found to catalyze the production of four luteolin glucuronides, including three known monoglucuronides and a novel 3′, 4′-diglucuronide. Ko143, a potent specific inhibitor of BCRP, significantly inhibited efflux of luteolin monoglucuronides from HeLa1A9 cells and increased their intracellular levels in a dose-dependent manner. The formation of luteolin diglucuronide was observed when intracellular concentration of total monoglucuronides went above 0.07 nM.

Conclusions Intracellular accumulation of diglucuronide was detected at high monoglucuronide concentrations (>0.07 nM). Diglucuronide production is speculated to be a compensatory pathway for luteolin disposition.

L. Tang • M. Hu • Z.-Q. Liu (✉)
International Institute for Translational Chinese Medicine
Guangzhou University of Chinese Medicine
Guangzhou, Guangdong, China 510006
e-mail: liuzq@smu.edu.cn

L. Tang • Y. Li • W.-Y. Chen • S. Zeng • L.-N. Dong • X.-J. Peng • M. Hu • Z.-Q. Liu
Department of Pharmaceutics, School of Pharmaceutical Sciences
Southern Medical University, Guangzhou, Guangdong, China 510515

W. Jiang • M. Hu
Department of Pharmacological and Pharmaceutical Sciences
College of Pharmacy, University of Houston 1441 Moursund Street
Houston Texas 77030, USA

KEY WORDS BCRP · glucuronidation · HeLa cells · luteolin · UGT1A9

INTRODUCTION

Luteolin, a well-known flavonoid polyphenolic compound, is found in many plant groups including Bryophyta, Pteridophyta, Pinophyta, and Magnoliophyta. Dietary sources of luteolin include carrots, peppers, celery, olive oil, peppermint, thyme, rosemary, and oregano (1). Luteolin is thought to have diverse beneficial biological effects such as cardioprotective, antioxidant, anti-inflammatory, and anticancer (1–3), and is a popular ingredient in nutritional supplements.

The pharmacological effects of luteolin, however, are severely limited by its low bioavailability resulting from extensive glucuronidation by human UDP-glucuronosyltransferases (UGTs) (4). Several groups have reported intestinal absorption and metabolism of luteolin in rats and humans and found that monoglucuronides were the main metabolites in rat plasma and human serum (5–7). Marelle *et al.* reported three glucuronidated luteolin metabolites, among which 7-O-glucuronosyl and 3′-O-glucuronosyl conjugates of luteolin were two major metabolites and 4′-O-glucuronosyl conjugate of luteolin was the third, minor metabolite (4). However, that study only reported the percentages of metabolites formed using nine UGT isoforms based on the peak area of luteolin and its metabolites, which hindered the determination of metabolic rates of each glucuronide.

Cellular glucuronidation of luteolin is affected by the activities of the glucuronidation enzymes, relevant efflux transporter and interplay between specific UGT isoforms and relevant efflux transporters. The latter is because glucuronides are too polar to passively diffuse out of cells, and need the action of relevant efflux transporters to exit the cells. The efflux transporters include breast cancer resistance protein

(BCRP), multidrug-resistance related protein 2 and 3 (MRP2 and MRP3).

BCRP, a plasma membrane efflux pump, was originally known to render multidrug resistance to chemotherapeutic agents such as mitoxantrone, camptothecins, anthracyclines, and flavopiridol (8). More recent studies have also shown that BCRP is involved in the intestinal and/or biliary excretion of many flavonoid glucuronides (9–11). Therefore, understanding the role of BCRP is important for assessing the contribution of BCRP to luteolin/glucuronide disposition and/or in determining the rate-limiting step (metabolism *vs.* excretion) in cellular glucuronide production.

Interplay between transporters and phase II drug-metabolizing enzymes appears to play a major role in phase II disposition of xenobiotics, especially flavonoids. However, effects of such interplay on luteolin disposition are not yet available as a suitable model for this purpose was lacking. Caco-2 and Madin-Darby canine kidney (MDCK) II cells, two cellular models most commonly used to delineate the interplay are still too complex for us to study the interplay between UGTs and efflux transporters. This is because multiple efflux transporters and other phase II enzymes (*e.g.*, SULTs) are also functionally expressed in these cells. Hence, this paper used recently established HeLa-UGT1A9 cells with one dominant UGT (UGT1A9) and one dominant efflux transporter (BCRP) (12,13) to investigate the metabolism of luteolin and excretion of its glucuronide metabolites. This cell allows the study of how interplay between a single UDP-glucuronosyltransferase isoform (UGT1A9) and a single efflux transporter (BCRP) affects luteolin disposition. This is because UGT1A9, a hepatic UGT, is the main UGT isoenzyme involved in biotransformation of luteolin to monoglucuronides (4).

Theoretically, luteolin, which has four hydroxyl groups, can be metabolized to monoglucuronides and diglucuronides *via* UGTs. However, no luteolin diglucuronides were discovered *in vitro* using the UGT reaction system that many people employs. However, direct and indirect evidence has suggested that UGTs are capable of producing diglucuronide of xenobiotics and endogenous compounds. For example, 4′,7-diglucuronide of genistein was found to be one of the major metabolites in human plasma after dietary administration of *kinako* (baked soybean powder, mainly contain genistein and daidzein) (14). Endogenous substances may also form diglucuronides. For example, bilirubin is known to be biotransformed into bilirubin monoglucuronide and diglucuronide by hepatic UGT1A1, and the resulting glucuronides is excreted into bile for elimination (15). The purpose of our current study is to show if luteolin could be metabolized to diglucuronide in HeLa-UGT1A9 cells. The research will shed lights on how efflux kinetics (*i.e.*, rate of glucuronide formation and glucuronide efflux) and effect of BCRP-UGT1A9 interplay affect luteolin glucuronidation and types of metabolites formed *in vivo*.

MATERIALS AND METHODS

Materials

HeLa cells, HeLa cells stably transfected with UGT1A9 (HeLa-UGT1A9 cells) and Ko143 were provided by Dr. Ming Hu (Department of Pharmacological and Pharmaceutical Sciences, College of Pharmacy, University of Houston, Houston, Texas, USA). Luteolin (≥98%, HPLC grade) and carvacrol (≥99%) were purchased from Shanghai Aladdin Reagent Company (Shanghai, China). Glucose, $NaHCO_3$, Hank's balanced salt solution (HBSS; powder form), uridinediphosphoglucuronic acid, alamethicin, D-saccharic-1, 4-lactone monohydrate and magnesium chloride were purchased from Sigma-Aldrich Co. (St. Louis, MO, USA). Human liver microsomes and expressed UGTs (Supersomes ™) were purchased from BD Biosciences (Woburn, MA, USA). HyClone fetal bovine serum and HyClone penicillin-streptomycin solution were purchased from Thermo Fisher Scientific (MA, USA). Bradford protein assay kit was bought from Bio-Rad (Hercules, CA, USA). All other chemicals and solvents were of analytical grade or better and used as received.

Cell Culture and Preparation of Cell Lysate

HeLa cells and HeLa-UGT1A9 cells were cultured in Dulbecco' modified Eagle's medium (DMEM) containing 10% fetal bovine serum, 100 U/mL penicillin and 100 μg/mL streptomycin according to previously published procedures (12). The cells were grown at 37°C under 5% CO_2 and 90% relative humidity. The cell lysate was prepared as previously described (16). In brief, the cell monolayers grown for 3 days to 4 days in flasks were washed twice with 37°C HBSS, gathered in 50 mM of potassium phosphate buffer (pH 7.4), and then ultra-sonicated in an ice bath for 30 min. The cell lysates were centrifuged at 6,000 rpm for 5 min at 4°C. The supernatant was harvested for UGT activity assay. The protein concentration of the cell lysates was determined using Bradford protein assay kit.

Enzymatic Activities of Expressed UGTs

The UGT reaction was performed as previously described (17). Briefly, UGT1A9 or other UGT isoforms (final concentration = 0.0053 to 0.26 mg protein/ml), magnesium chloride (0.88 mM), D-saccharic-1,4-lactone monohydrate (4.4 mM), alamethicin (0.022 mg/ml), 1 mM substrate in a 50 mM potassium phosphate buffer (pH 7.4), and uridine 5′-diphospho-glucuronic acid or UDPGA (3.5 mM, added last) were mixed. The mixture with a final volume of 120 μl was incubated at 37°C for a predetermined period of time. The reaction was stopped by the addition of 60 μl methanol

containing 0.5 ng/ml propiophenone (defined as "stop solution") as the internal standard. All experiments were performed in triplicates. The samples were centrifuged at 13,000 rpm for 30 min, and 10 μl of the supernatant were then analyzed by ultra-performance liquid chromatography (UPLC) or liquid chromatography-mass spectrometry (LC/MS).

UGT1A9 Inhibitor Experiment in Human Liver Microsomes (HLMs) and UGT1A9

Carvacrol was used as the inhibitor of UGT1A9 in HLMs and expressed UGT1A9 to determine the major isoforms responsible for luteolin glucuronidation (18). The concentration of luteolin was 10 μM and the final concentration of HLMs and UGT1A9 were 0.26 mg protein/ml. UGT1A9 or HLMs, magnesium chloride (0.88 mM), sccharadacton (4.4 mM), alamethicin (0.022 mg/ml), 1 mM substrate in a 50 mM potassium phosphate buffer (pH=7.4) were mixed and the carvacrol was added and mixed well. After 5 min preincubation at 37°C, the UDPGA was added in the mixture to initiate the reaction. The incubation time was 60 min. The final concentrations of carvacrol were 50, 100 and 200 μM. The control group was absence of carvacrol. After precipitating protein by methanols containing propiophenone (stop solution) and centrifugating (30 min at 13,000 rpm), samples were selected for UPLC analysis.

Glucuronidation of Luteolin in Cell Lysate and UGT1A9

Incubation was carried as described above. The final concentration of the cell lysate was 0.494 and 0.1 mg/ml to UGT1A9, respectively. Different concentrations of luteolin (0.5 μM to 40 μM) were selected, and the incubation time was 30 min. At the end of the reaction, the incubation samples were mixed with the stop solution and analyzed by UPLC after centrifugation at 13,000 rpm for 30 min.

Glucuronide Excretion Experiments in the HeLa-UGT1A9 Cell Model

We quantified the excretion glucuronides of luteolin from HeLa-UGT1A9 using a previously reported method (10). HeLa-UGT1A9 cells were seeded onto six-well plates at a concentration of 1×10^5 cell/well and cultured for 3 days to 4 days. Before the experiments, the culture medium was moved, and each well was washed twice with 2 ml HBSS at 37°C. Subsequently, 2 ml HBSS containing different luteolin concentrations (1, 2, 5, 10, 20, and 40 μM with 0.1% DMSO) was added to each well. At 20, 40, and 60 min, 0.5 ml of incubation medium from each well were collected, and the same volume of luteolin solution was loaded in each well. The times were selected to ensure that the amount *versus* time plots stay in the linear range. For the experiment that determines whether the concentration of glucuronides was a factor of diglucuronide formation, a protein inhibitor of breast cancer resistance, protein-Ko143, was used. Ko143 (5 or 10 μM) was diluted in a solution containing luteolin (2, 10, and 40 μM). At intervals of 30, 60, and 80 min, approximately 0.5 ml of incubation medium was selected from each well, and the same volume of medium containing Ko143 and lutelion was used to replenish each well. The samples were mixed with a stop solution and were prepared for UPLC analysis after centrifugation at 13,000 rpm for 30 min.

Determination of Intracellular Metabolites of Luteolin in HeLa-UGT1A9

After the excretion experiment, the cells were washed twice with ice-cold HBSS, and the selected cells in 200 μl HBSS buffer were ultrasonicated in an ice bath for 10 min at maximum power. After centrifugation at 13,000 rpm for 30 min, the supernatant was obtained, mixed with the stop solution, and then prepared for UPLC analysis after centrifugation at 13,000 rpm for 30 min.

LC/MS^n and UPLC Analysis of Luteolin and Its Metabolites

A quadrupole-time of flight tandem mass spectrometer (Bruker, USA) with an Agilent HPLC was used to determine the molecular weight of luteolin and its metabolites. The conditions were as follows: column, Agilent ZORBAX SB-C18, 5 μm, 4.6 mm×150 mm; mobile phase B, 100% acetonitrile, mobile phase A, 100% aqueous buffer (0.1% formic acid); flow rate, 1 ml/min; gradient, 0 min to 9 min, 95% to 65% A, 9 min to 13 min, 65% to 50% A, 13 min to 15 min, 50% to 95% A, wavelength, 340 nm; and injection volume, 200 μl. Ionization was achieved using electrospray ionization in the positive mode at a capillary voltage of 4,500 V. The temperature of the dry heater was maintained at 200°C, and the nebulizer voltage was set at 1.5 bars. The dry gas was set at a flow rate of 8.0 l/min. The MS/MS spectra were produced by collision-induced dissociation of the selected precursor ions. Data were collected and analyzed using Bruker Daltonics software (version 4.0, Bruker, USA).

An Acquity UPLC system (Premier XE, Waters Corp., Milford, MA, USA) with photodiode array detector and Empower software was used for the quantification of luteolin metabolites. The conditions were as follows: column, HSS T3, 1.8 μm, 2.1 mm×100 mm; mobile phase B, 100% acetonitrile, mobile phase A, 100% aqueous buffer (0.1% formic acid); flow rate, 0.3 ml/min; gradient, 0 min to 5 min, 95% to 45% A, 5 min to 5.5 min, 45% to 30% A, 5.5 min to 6 min, 30% to 90% A, 6 min to 6.5 min, 90% to 95% A, wavelength, 340 nm for luteolin and its glucuronides and 240 nm for propiophenone; injection volume, 10 μl.

Determination of Molar Extinction Coefficient Ratio for Each Glucuronide and Its Conjugation Position

For quantification of each metabolite, the conversion factor (K), which represents the ratio between the molar extinction coefficient of each glucuronide and luteolin, was determined following a previously described method (19). To calculate the conversion factor K, each metabolite was separated by HPLC, collected for blow drying in air, dissolved with KPI, and then divided into two parts, one of which was analyzed directly and the other was analyzed after being hydrolyzed with β-glucuronidase (100 units/ml) at 37°C for 2 h. The difference in the amount of aglycones found in these two samples was the amount of metabolites formed. The relationship between the peak areas of the metabolites before hydrolysis and the peak areas of aglycones after the hydrolysis was used to establish the conversion factor needed to quantify the amounts of luteolin conjugates. In accordance with the previous finding (4), we defined three monoglucuronides. To determine the conjugation position of diglucuronide (M-2G), the metabolite was separated, collected, and then hydrolyzed with β-glucuronidase for 1 h to ensure that M-2G was not hydrolyzed completely and could produce two related monoglucuronides. The retention time of the metabolite is a determinant for the conjugation position of luteolin (*e.g.*, M-2G).

Kinetic Analysis

The metabolic rates by UGT Supersome™ and cell lysate of HeLa-UGT1A9 were expressed as the amount of metabolites formed (nmol/min/mg). Kinetic parameters were then obtained based on the fit to various kinetic equations as described below, aided by profiles of the Eadie-Hofstee plots as previously described (20). When the Eadie-Hofstee plots were linear, the data fitted the standard Michaelis- Menten equation:

$$V = \frac{V_{max} C}{K_m + C} \tag{1}$$

where V_{max} is the maximal formation rate and K_m is the substrate concentration required to achieve 50% of V_{max}. If the Eadie-Hofstee plots showed the characteristic profiles of atypical kinetics, the data were fitted to other corresponding equations (21).

Calculation of Excretion Rates, f_{met} Value, and Clearance of Efflux Transporter

The excretion rates of glucuronides were calculated as the slope of amounts *versus* time curves. The fraction of the metabolized dose (f_{met}) calculated in this study reflects the extent of metabolism in the presence of transporter-enzyme interplay (22).

$$f_{met} = \frac{\sum \text{metabolites}}{\sum \text{metabolites} + \sum \text{parent compound}} \tag{2}$$

Clearance of efflux transporter (CL) was calculated in this study because the extracellular concentration of glucuronides can be different with their intracellular concentration. CL was determined using the excretion rate of glucuronides ($\mathcal{J}$) divided by the intracellular concentration of glucuronide (Ci):

$$Cl = \frac{\mathcal{J}}{Ci} = \frac{\mathcal{J}max}{Km + Ci} \tag{3}$$

where $\mathcal{J}max$ is the maximal excretion rate of glucuronide and Km is the Michaelis constant of glucuronide efflux. In deriving the Ci, we assumed that the average cytosolic water volume of the HeLa-UGT1A9 cells was 4 µl/mg proteins, as was done previously (23). The intracellular metabolite concentration was calculated from the total amount of intracellular glucuronides divided by the total volume of intracellular proteins (24).

Statistical Analysis

All experiments were conducted in triplicate. One-way ANOVA with or without Tukey-Kramer multiple comparison and Student's *t*-test were used to evaluate statistical difference. Differences were considered significant at $p < 0.05$ or $p < 0.01$.

RESULTS

Identification of Luteolin Glucuronides

Four metabolites (M1-3 and M-2G) with different retention times were identified in UPLC analysis (Fig. 1a). Metabolites M1, M2, and M3 all showed a pseudo-molecule ion $[M+H]^+$ of m/z 463.0871 in full-scan mass spectra (Fig. 1b), indicating that they had the molecular formula of $C_{12}H_{19}O_{12}$. According to previously published data (4), metabolites M1, M2, and M3 were identified to be luteolin-7-O-glucuronide, luteolin-4′-O-glucuronide, and luteolin-3′-O-glucuronide, respectively. M-2G (Fig. 1a) showing pseudo-molecular ion $[M+H]^+$ of m/z 639.1192 (Fig. 1b), was a new metabolite that had not been reported previously. The pseudo-molecular ion $[M+H]^+$ of m/z 639.1192 and fragment ions at m/z 463 and 287 (data not shown) indicated that M-2G had the

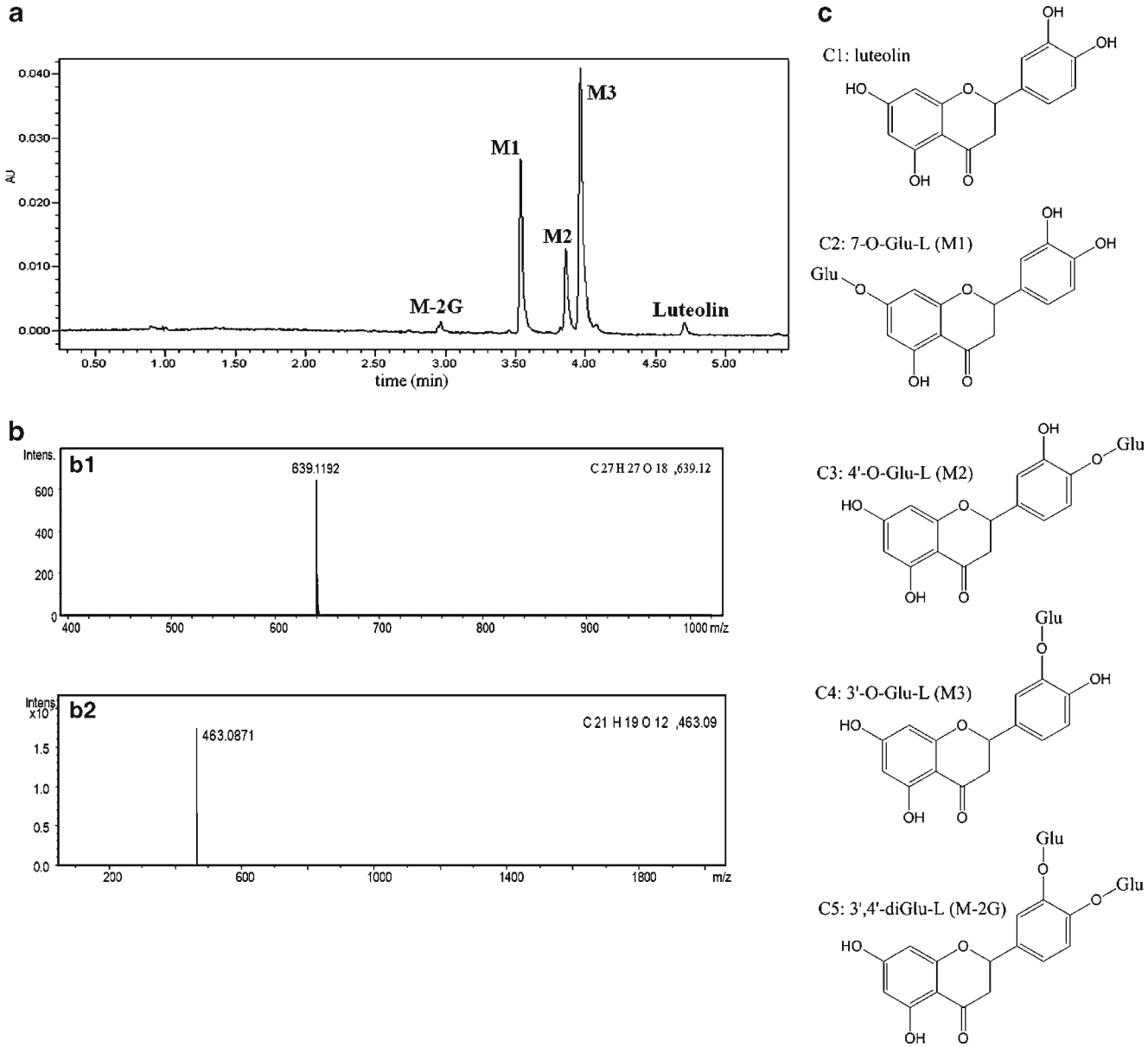

Fig. 1 UPLC and HRMS profiles of luteolin and its metabolites with the structures of the metabolites. UPLC was used to separate and quantify luteolin and its metabolites in the experimental samples generated after incubation with human UGT1A9 supersomes. (**a**) Chromatograms of the luteolin, internal standard (*IS*), and the flavone's respective metabolites. HRMS was used to identity of the metabolites as diglucuronide and monoglucuronides of luteolin. (**b**) HRMS scan for the diglucuronide and monoglucuronide.

molecular formula of $C_{27}H_{27}O_{18}$, suggesting that it was a diglucuronide. UPLC and HPLC retention times and parameters of the QTOF tandem mass spectrometer were summarized in Table I.

Table I Retention Time of Luteolin and Its Four Metabolites in UPLC and HPLC Chromatograms with the HRMS Date

	UPLC t_R (min)	HPLC t_R(min)	$[M+H]^+$(m/z)	Molecular formula
2Glu-L-O-′	2.989	4.8	639.1234	$C_{27}H_{27}O_{18}$
7-O-Glu-L′	3.598	5.4	463.0907	$C_{21}H_{19}O_{12}$
4'-O-Glu-L	3.892	5.7	463.0902	$C_{21}H_{19}O_{12}$
3'-O-Glu-L	3.952	5.9	463.0902	$C_{21}H_{19}O_{12}$
Luteolin'	4.647	6.5	287.0560	$C_{15}H_{10}O_6$

Molar Extinction Coefficient Ratio for Each Glucuronide and Conjugation Position of Diglucuronide

M-2G hydrolysis generated two monoglucuronides (M2 and M3) and luteolin, indicating that M-2G was a 3′, 4′-diglucuronide. The conversion factors of M1-M3 and M-2G were 3.63±0.13, 6.36±0.35, 5.74±0.77, and 3.72±0.31, respectively.

Luteolin Glucuronidation by 12 Human Expressed UGT Isoforms

Our results indicated that while UGT1A1, UGT1A7, UGT1A8, UGT1A9, and UGT1A10 all catalyzed formation of diglucuronide, UGT1A9 showed the highest activity in diglucuronide production (Fig. 2A1). All UGT isoforms catalyzed biotransformation of luteolin to M1 except UGT1A4 and UGT2B4, and UGT1A9 was the most active among these 12 isoforms (Fig. 2A2). As for luteolin conversion to M2, all isoforms showed activity except UGT1A4, and UGT1A1, UGT1A8, UGT1A9, and UGT1A10 were ranked as the top four in activity (Fig. 2A3). M3 metabolite formation was catalyzed by UGT1A1, UGT1A3, UGT1A7, UGT1A8, UGT1A9, UGT1A10, and UGT2B7, with UGT1A9 again being the most active among all the UGT isoforms tested (Fig. 2A4).

Effects of UGT1A9 Inhibitior on Luteolin Metabolism

Carvacrol, a selective inhibitor of UGT1A9 was used to determine how much UGT1A9 contributed to luteolin metabolism in phase II reaction system in human liver microsomes (HLMs). Carvacrol inhibited M1, M2, M3 and M-2G production in phase II reaction systems in both HLMs and expressed UGT1A9 in a dose-dependent manner. 200 μM of carvacrol inhibited M1, M2, M3 and M-2G generation approximately by 44.3%, 17.6%, 53.2% and 56.7% in HLMs and 59.8%, 34.6%, 79.2% and 83.4% in recombinant UGT1A9, respectively (Fig. 2b). The time course of luteolin metabolism was also studied. When 10 μM luteolin was incubated for 30, 60, 90, and 120 min with 0.26 mg/ml UGT1A9 (final concentration), M-2G level increased linearly with time (Fig. 2c), whereas M2 level decreased with time after 30 min ($p < 0.01$).

Enzyme Kinetic Study in HeLa1A9 Cells and Expressed UGT1A9

UGT1A9 expression in HeLa1A9 cells was confirmed by western blot analysis (12). It was found that UGT1A9 level in Supersomes™ expressing human UGT1A9 was 6.3-fold of that in HeLa1A9 cell lysate with the same amount of total proteins. Luteolin metabolism catalyzed by UGT1A9 from the two sources followed the classic Michaelis-Menten equation. K_m, V_{max}, and CL (V_{max}/K_m) values obtained from these kinetic studies were summarized in Table II, and rate *versus* concentration plots were shown in Fig. 3. In general, K_m values of M1, M2, and M3 were similar between the two UGT1A9 sources. V_{max} values of UGT1A9 were also similar between the two sources except V_{max} for M1 production, which was much higher in HeLa1A9 cell lysate than that in expressed UGT1A9.

Fig. 2 Glucuronidation of luteolin by 12 Expressed Human UGTs (**a**), UGT1A9 inhibitor experiment in HLMs and UGT1A9 (**b**) and kinetics of M-2G production (**c**). Luteolin metabolites in 12 expressed human UGTs (*A1*, *A2*, *A3* and *A4*) include one di-glucuronide (M-2G, *A1*) and three mono-glucuronides (M1, M2, M3, *A2–A4*) at 10 μM when the inhibition time was 30 min. Inhibitory effects of carvacrol on luteolin glucuronidation in HLMs and UGT1A9 were shown in (**b**). Luteolin (10 μM) was incubated with HLMs and UGT1A9 (0.053 mg of protein/ml) at 37°C for 30 min in the absence or presence of carvacrol (0 μM to 200 μM). Luteolin (10 μM) was incubated for different times with UGT1A9 (0.26 mg of protein/ml) to determine the kinetics of M-2G production (**c**). Data represent the mean and S.D. of three determinations.

Effects of Luteolin Concentration on Glucuronide Excretion

The effect of luteolin concentration on the excretion, intracellular amount, clearance (CL), and f_{met} of monoglucuronides were studied at six concentrations (Fig. 4). Excretion rates of M1, M2, and M3 increased with luteolin concentration within the range of 1 μM to 5 μM, reached a plateau at 5 μM, and started to decrease at 20 μM (Fig. 4a). In contrast, intracellular monoglucuronide levels increased with luteolin loading concentrations (Fig. 4b). Interestingly, intracellular monoglucuronide concentrations increased faster than the increase in luteolin loading concentration, likely attributed to the significant decrease in cellular clearance of the three monoglucuronides at higher concentrations (Fig. 4c). In addition, f_{met} decreased with increasing luteolin concentration (Fig. 4d).

Effect of Ko143 on Intracellular Glucuronides and Formation of M-2G

At the 2 μM luteolin loading concentration, three intracellular monoglucuronides were observed with or without the use of Ko143, and no diglucuronides were found. Compared with control sample (without Ko143), intracellular samples showed 2.5- and 1.4-fold increase in M2 and M3 levels in the presence of 5 μM Ko143

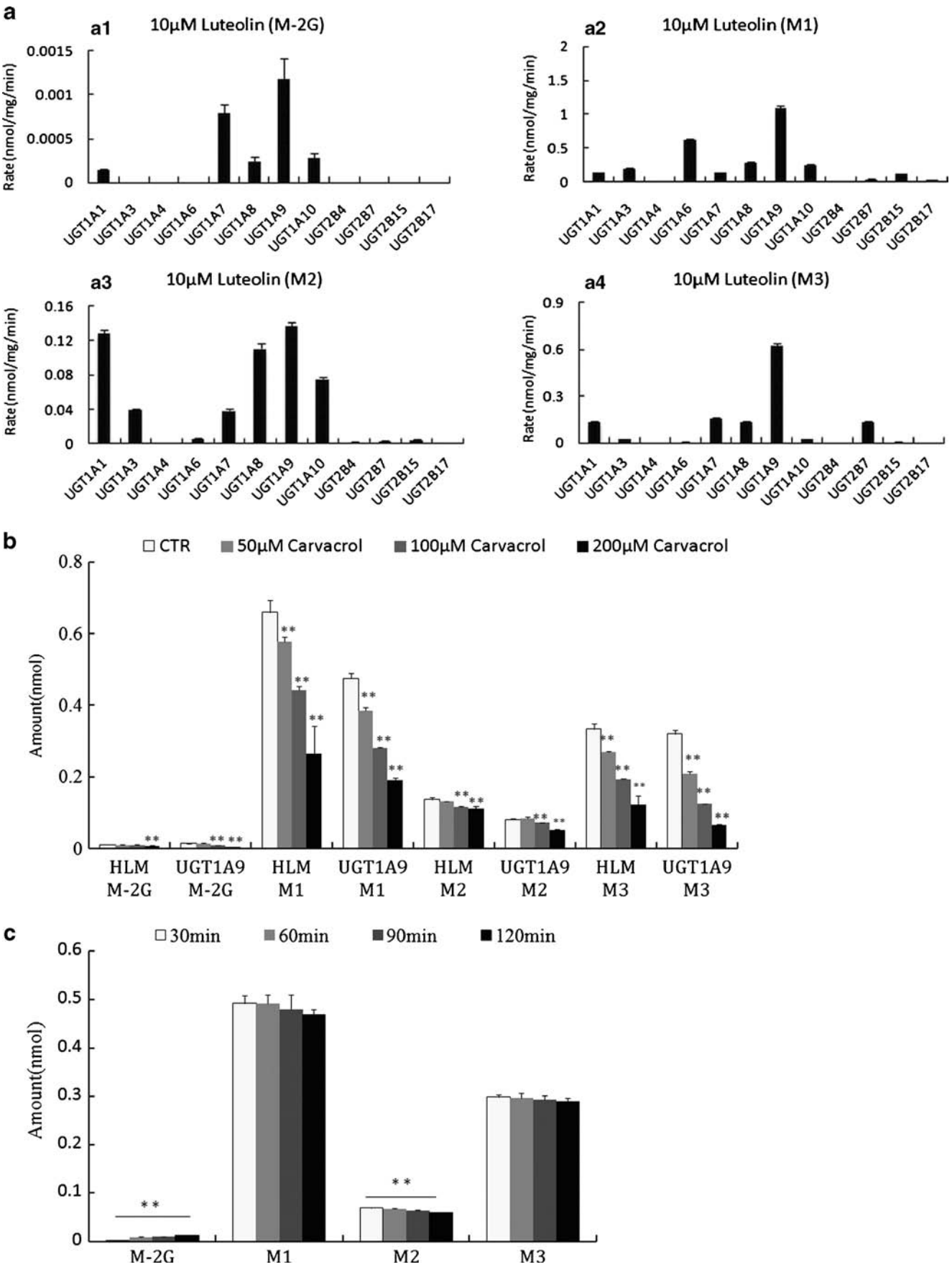
a
a1
10μM Luteolin (M-2G)
Rate (nmol/mg/min)
0.0015
0.001
0.0005
0
UGT1A1 UGT1A3 UGT1A4 UGT1A6 UGT1A7 UGT1A8 UGT1A9 UGT1A10 UGT2B4 UGT2B7 UGT2B15 UGT2B17
a2
10μM Luteolin (M1)
Rate (nmol/mg/min)
2
1.5
1
0.5
0
UGT1A1 UGT1A3 UGT1A4 UGT1A6 UGT1A7 UGT1A8 UGT1A9 UGT1A10 UGT2B4 UGT2B7 UGT2B15 UGT2B17
a3
10μM Luteolin (M2)
Rate (nmol/mg/min)
0.16
0.12
0.08
0.04
0
UGT1A1 UGT1A3 UGT1A4 UGT1A6 UGT1A7 UGT1A8 UGT1A9 UGT1A10 UGT2B4 UGT2B7 UGT2B15 UGT2B17
a4
10μM Luteolin (M3)
Rate (nmol/mg/min)
0.9
0.6
0.3
0
UGT1A1 UGT1A3 UGT1A4 UGT1A6 UGT1A7 UGT1A8 UGT1A9 UGT1A10 UGT2B4 UGT2B7 UGT2B15 UGT2B17
b
CTR
50μM Carvacrol
100μM Carvacrol
200μM Carvacrol
Amount(nmol)
0.8
0.6
0.4
0.2
0
HLM M-2G
UGT1A9 M-2G
HLM M1
UGT1A9 M1
HLM M2
UGT1A9 M2
HLM M3
UGT1A9 M3
c
30min
60min
90min
120min
Amount(nmol)
0.6
0.5
0.4
0.3
0.2
0.1
0
M-2G
M1
M2
M3

Table II Kinetic Parameters of Luteolin Glucuronidation in UGT1A9 and HeLa1A9

		UGT1A9	HeLa-U1A9
M1($K = 3.63 \pm 0.13$)	Km(μM)	3.97 ± 0.51	3.29 ± 0.24
	Vmax(nmol·min^{-1}·mg^{-1})	8.88 ± 0.33	13.32 ± 0.32
	CL	2.23	4.05
	AIC	−0.32	−35.68
	R2	0.97	0.99
M2($K = 6.36 \pm 0.35$)	Km(μM)	2.02 ± 0.36	1.88 ± 0.071
	Vmax(nmol·min^{-1}·mg^{-1})	1.33 ± 0.049	1.43 ± 0.015
	CL	0.66	0.76
	AIC	−26.52	−98.41
	R2	0.97	0.99
M3($K = 5.74 \pm 0.77$)	Km(μM)	1.93 ± 0.28	1.53 ± 0.12
	Vmax(nmol·min^{-1}·mg^{-1})	5.11 ± 0.15	6.00 ± 0.12
	CL	2.65	3.92
	AIC	−8.26	−51.01
	R2	0.95	0.99
M-2G ($K = 3.72 \pm 0.31$)			

K The conversion factors of mono-glucuronidations and diglucuronide

while showed 4.3- and 2.4-fold increase in M2 and M3 levels in the presence of 10 μM Ko143. However, no significant increase in M1 was observed in the presence of Ko143 (Fig. 5a). At 10 μM, amounts of intracellular M1, M2, and M3 increased by 1.7-, 1.5-, and 1.8-fold in the presence of 5 μM Ko143, and 3.1-, 3.7-, and 3.9-fold in the presence of 10 μM Ko143, respectively. Although no M-2G was detected in the absence of Ko143, M-2G concentrations were determined to be 0.041 and 0.086 nmol in the presence of 5 and 10 μM Ko143, respectively (Fig. 5b). At 40 μM luteolin loading concentration, no significant differences in the intracellular amount of the four glucuronides were found between the control group and the 5 μM Ko143 group. In the presence of 10 μM Ko143, intracellular M1, M2, and M3 levels increased by 2.2-, 3.0-, and 2.7-fold, respectively. And in comparison with control, the amount of M-2G increased by 3.3-fold in the presence of 10 μM Ko143 (Fig. 5c).

Effect of Ko143 on Glucuronide Excretion

Ko143 was used to determine the role of BCRP in the excretion of glucuronides in HeLa1A9 cells (Fig. 6). Previous studies reported that Ko143 had a Ki value below 1 μM (25). Thus, Ko143 was used at 5 and 10 μM for complete inhibition of BCRP. As expected, the rates of excretion of luteolin glucuronides decreased in the presence of Ko143 at 10 μM and 40 μM luteolin loading concentration. At 2 μM luteolin concentration, the sampling times cannot ensure the amount excreted *versus* time plot staying in a linear range and after 80 min incubation, 5 μM Ko143 inhibited M1 and M3 excretion both by 12% and 10 μM Ko143 by 20% and 18%, respectively (Fig. 6a).

Effect of Ko143 on the Total Amount of Glucuronides, f_{met}, and CL

The effect of Ko143 on the total intracellular amount of monoglucuronides was shown in Fig. 7a. At 2 and 10 μM luteolin concentrations, the total amounts of monoglucuronide metabolites increased by 1.4- and 1.8-fold in the presence of 5 μM Ko143, and by 2.1- and 3.6-fold in the presence of 10 μM Ko143, respectively, compared with the control (Fig. 7A1 and A2). At 40 μM luteolin concentration, the total amount of monoglucuronide metabolites increased by 2.5-fold in the presence of 10 μM Ko143 compared with the control (Fig. 7A3). The effect of Ko143 on the total amount of extracellular glucuronides was demonstrated in Fig. 7b. At three luteolin concentrations, the total amounts of extracellular glucuronides all decreased in the presence of 5 μM and 10 μM Ko143. However, further data analysis indicated that the effect of Ko143 on luteolin glucuronidation was small or insignificant, as shown in the moderate decreases in f_{met} (Fig. 7c). Compared with its limited effect on f_{met}, Ko143 drastically inhibited cellular clearance (CL) of the three monoglucuronides (Fig. 7d). For example, at 10 μM luteolin concentration, CL of M1, M2, and M3 decreased by 65% ($p < 0.01$), 63% ($p < 0.05$), and 65% ($p < 0.01$) in the presence of

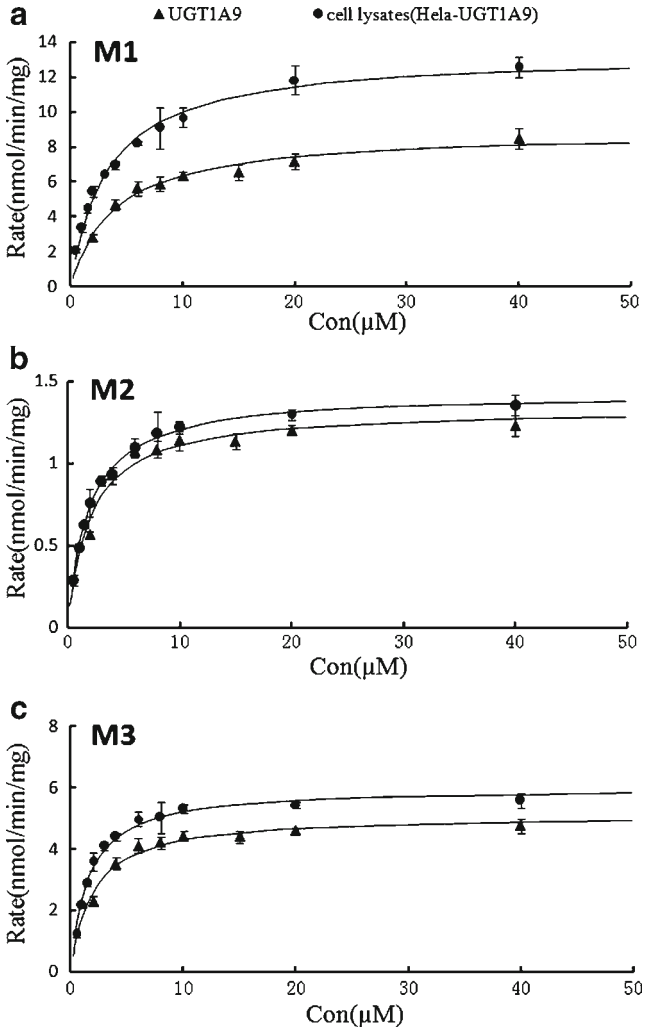

Fig. 3 Kinetics of luteolin glucuronidation by expressed UGT1A9 isoforms and UGT1A9 overexpressed in HeLa cells. The glucuronidation rates by expressed UGT1A9 and cell lysates were determined at concentration ranges of 2 μM to 40 μM and 0.5 μM to 40 μM, respectively, within 30 min of reaction time. M1 to M3 represent the curves of the three monoglucuronide metabolites (**a–c**). The curves are estimated based on fitted parameters generated using the Michaelis-Menten equation. Each data point was the average of three determinations with error bars representing S.D. The apparent kinetic parameters are listed in Table II.

5 μM Ko143, and by 84% ($p<0.01$), 77% ($p<0.01$), and 77% ($p<0.01$) in the presence of 10 μM Ko143, respectively (Fig. 7D1).

DISCUSSION

The present study provided direct evidence that UGT1A9 is the main UGT isoform that catalyzes the metabolism of luteolin in human liver because carvacrol, a specific inhibitor of UGT1A9, significantly inhibited luteolin glucuronidation in human liver microsomes and expressed human UGT1A9. UGT1A9 was found to catalyze the production of four luteolin glucuronide metabolites, including three known monoglucuronides (4) and a new diglucuronide that had not been reported previously. Similar to what was reported previously (4), the three monoglucuronides were determined to be 7-, 4′-, and 3′-luteolin monoglucuronides (M1, M2, and M3) (Fig. 1). The diglucuronide metabolite was determined to be luteolin 3′, 4′-diglucuronide based on the observation that it was hydrolyzed to generate M2 and M3.

Among 12 human UGT isoforms, UGT1A1 and UGT1A9 are highly expressed in liver (26). Carvacrol, a specific UGT1A9 inhibitor dose-dependently inhibited the formation of M1 and M3 in human liver microsomes (HLMs), suggesting that UGT1A9 was the main UGT isoform responsible for the formation of M1 and M3 metabolites. Indeed, our results from cDNA-expressed UGT isoforms indicated that UGT1A9 was the most active among the 12 UGT isoforms in catalyzing the formation of M1 and M3. However, for M2 formation, UGT1A1, 1A3, 1A7, 1A8, 1A9 and 1A10 are all major isoforms (Fig. 2), which explained why carvacrol showed weaker dose-dependent inhibition of M2 formation in HLMs. Carvacrol inhibited M2 formation in HLMs by only 17% even at the highest dose of 200 μM (Fig. 2a). Our results also indicated that the production of diglucuronide in human liver microsomes might be a newly discovered pathway for luteolin clearance *in vivo*. Interestingly, unlike the production of the three monoglucuronides, which peaked within 30 min of incubation and remained stable thereafter, the production of diglucuronide increased slowly with incubation time (Fig. 2). To date, only a few endobiotics (*e.g.* bilirubin) and xenobiotics (*e.g.* 3, 6-quinol/chrysene-3, 6-quinol) have been reported to be metabolically converted to diglucuronides *in vitro* (27,28). For example, recombinant human UGT1A1 efficiently converts two bilirubin monoglucuronides to a diglucuronide (28), and bilirubin diglucuronide is the main form of bilirubin secreted in human bile. No flavonoid diglucuronides have been found *in vitro* although many flavonoid diglucuronides (*e.g.* daidzein and genistein diglucuronides) have been observed *in vivo*. In the present study, luteolin diglucuronide was detected after long incubation (>60 min) of luteolin with high concentration of UGT (0.26 mg/ml). We speculated that diglucuronide was produced by recombinant human UGTs when concentrations of monoglucuronides reached certain levels. In other words, formation of diglucuronides is a sequential process.

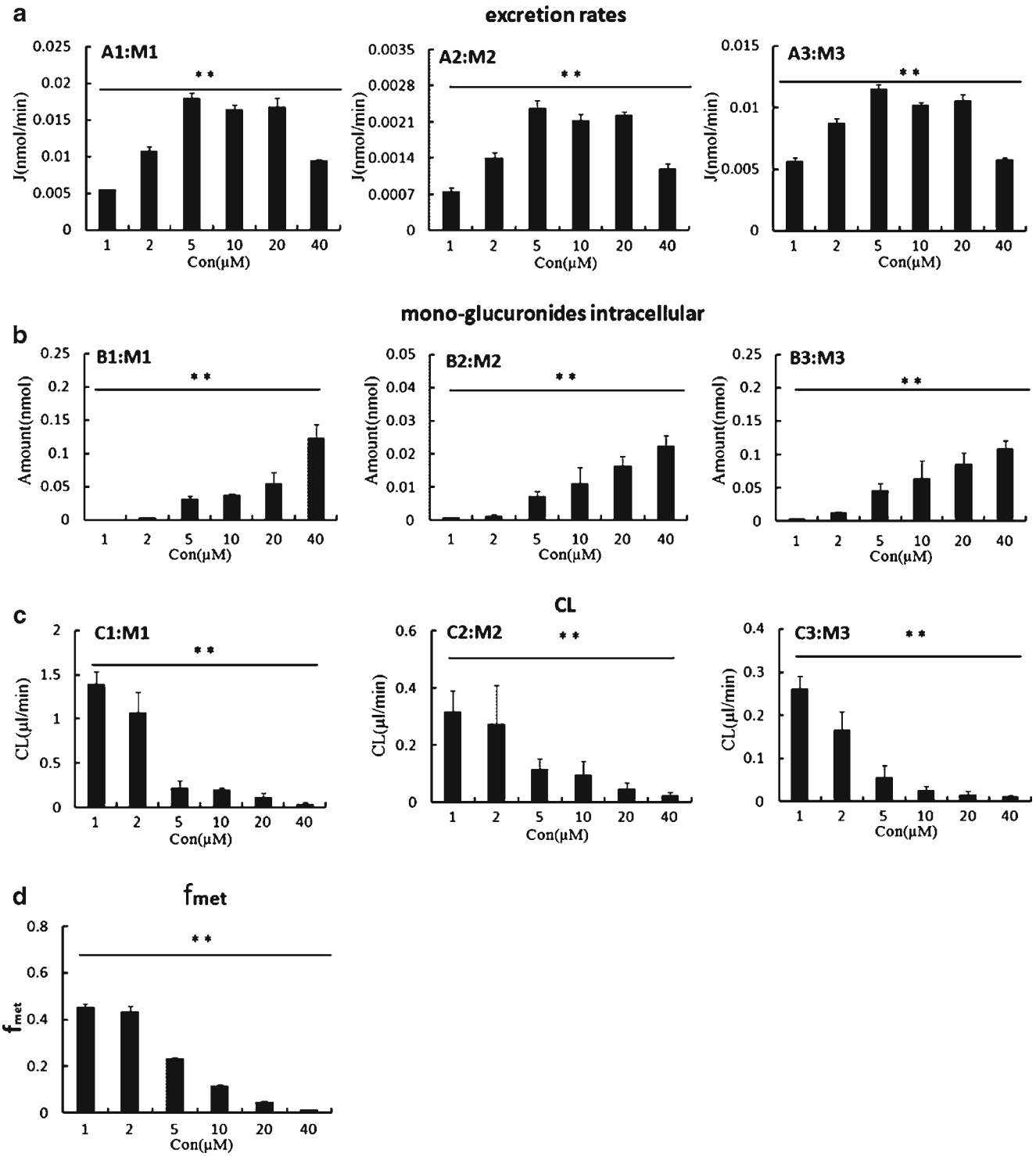

Fig. 4 Effects of concentrations on the excretion rates (**a**), intracellular amounts (**b**), and f_{met} (**c**) of three monoglucuronides (M1 to M3). Different concentrations of luteolin were incubated with UGT1A9 overexpressing HeLa cells grown on six-well plates (1×10^5 cells/well), and three samples (500 μl) were taken at 20, 40, and 60 min and replaced with fresh loading solution (500 μl) containing luteolin. The excretion rates of glucuronides were calculated as the slope of amounts *versus* time curves. The intracellular amounts of monoglucuronide were determined at the end of excretion experiment after the cells were washed thrice with ice-cold HBSS. Each data point is the average of three determinations, with error bar representing the S.D. ($n = 3$). **, $p < 0.01$.

HeLa cells overexpressing UGT1A9 (HeLa1A9) were utilized to further elaborate luteolin metabolism in terms of monoglucuronide and diglucuronide production. The excretion of luteolin in forms of monoglucuronides and

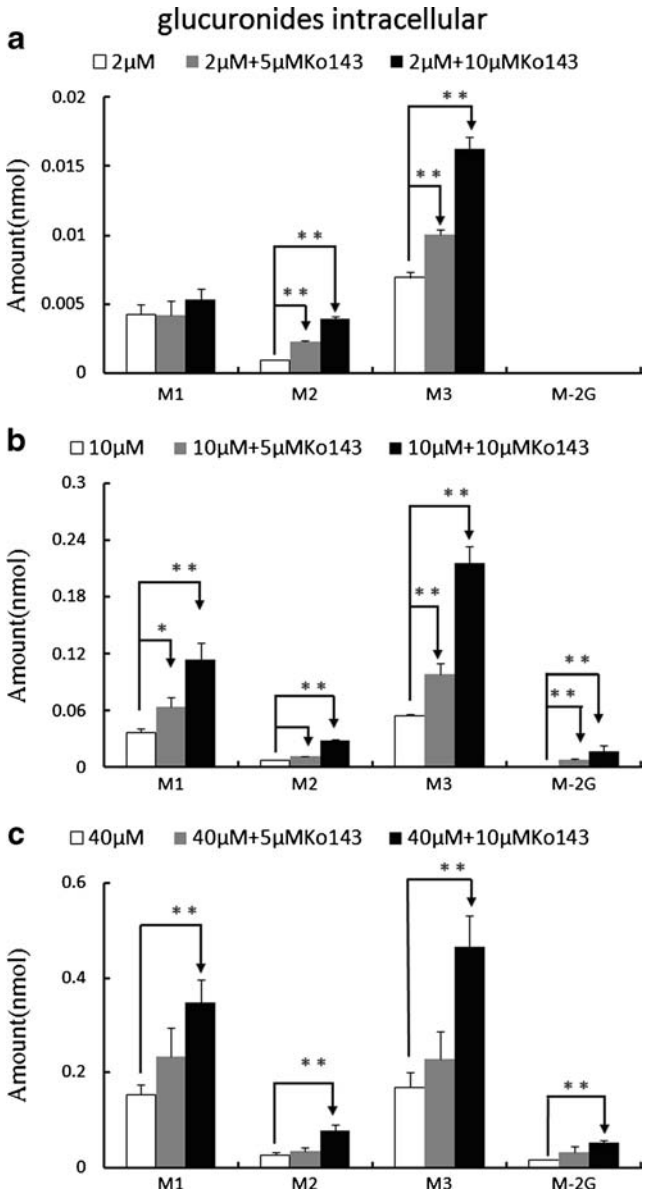

Fig. 5 Effect of the BCRP-specific inhibitor Ko143 on the intracellular amounts of the monoglucuronides (M1-G, M2-G, and M3-G) and diglucuronide (M-2G). Different concentrations of loading solution (2, 10, and 40 μM) (**a**–**c**), respectively. The intracellular amounts were determined at 80 min. Each data point is the average of three determinations, with error bar representing the S.D. ($n = 3$). *, $p < 0.05$; **, $p < 0.01$; *N.D.* not detectable; *CTR* control.

diglucuronide, was also analyzed. Our results showed that excretion of luteolin monoglucuronides in HeLa1A9 rapidly peaked at 5 μM luteolin concentration, remained stable at 10 and 20 μM, and then started to decrease at 40 μM. Because formation of glucuronides did not observe substrate inhibition kinetics, it was speculated that the decreased excretion rate of monoglucuronides at high luteolin concentration was most likely caused by BCRP inhibition by luteolin. Indeed, several flavonoids (*e.g.* retusin and ayanin) have been reported to inhibit BCRP encoded by the ABCG2 gene with potencies only slightly lower than that of Ko143. Structural features found to contribute positively to BCRP inhibition included a hydroxyl group in position 5 and double bond between position 2 and 3 (29), which were found in the structure of luteolin. Therefore, BCRP inhibition by luteolin was believed to account for the decreased excretion rate of monoglucuronides in HeLa-UGT1A9 cells observed at high luteolin concentrations.

The role of BCRP in the excretion of glucuronides was studied using Ko143, a specific BCRP inhibitor that does not affect UGT activities. Ko143 inhibited BCRP-mediated monoglucuronide excretion and increased accumulation of intracellular monoglucuronides in a dose-dependent manner (Fig. 5). Importantly, Ko143 also inhibited monoglucuronide clearance at multiple luteolin concentrations (2, 10, and 40 μM), suggesting that BCRP-mediated excretion was the predominant pathway for luteolin disposition. More importantly, Ko143 promoted the formation of diglucuronide at 10 μM luteolin, and significantly increased intracellular diglucuronide level at a higher luteolin concentration of 40 μM. It was found that diglucuronide was produced when total intracellular concentration of the three monoglucuronides (M1, M2, and M3) went over 0.07 nM, which was achieved in the presence of Ko143 or at a high luteolin concentration of 40 μM. Accumulating evidence suggests that UGTs are functional in ER membranes as dimeric complexes, and may form tetramers which are implicated in diglucuronide formation (30). Our observation that luteolin diglucuronide was detected in HeLa1A9, recombinant UGT1A9, and human liver microsomes suggested that UGT tetramers might exist in cellular ER membranes and the artificial UGT reaction system.

Interestingly, no diglucuronide was detected in the cultural medium of HeLa1A9, suggesting that BCRP-mediated diglucuronide efflux was inefficient and other efflux transporters might be involved in the cellular excretion of luteolin diglucuronide. Further research using more suitable models should provide insights into the mechanism of diglucuronide clearance. In addition, luteolin diglucuronidation by UGT1A9 was observed at much lower level compared with luteolin monoglucuronidations (Fig. 2a and b). Further investigation should be conducted to determine whether this novel diglucuronidation reaction takes place *in vivo*.

We found that kinetic characteristics of luteolin glucuronidation followed Michaelis-Menten model with UGT1A9 derived from HeLa1A9 cells or with the commercially available expressed UGT1A9. The K_m values were similar between UGT1A9 derived from HeLa1A9 cells and recombinant UGT1A9 ($p > 0.05$; Fig. 3). The

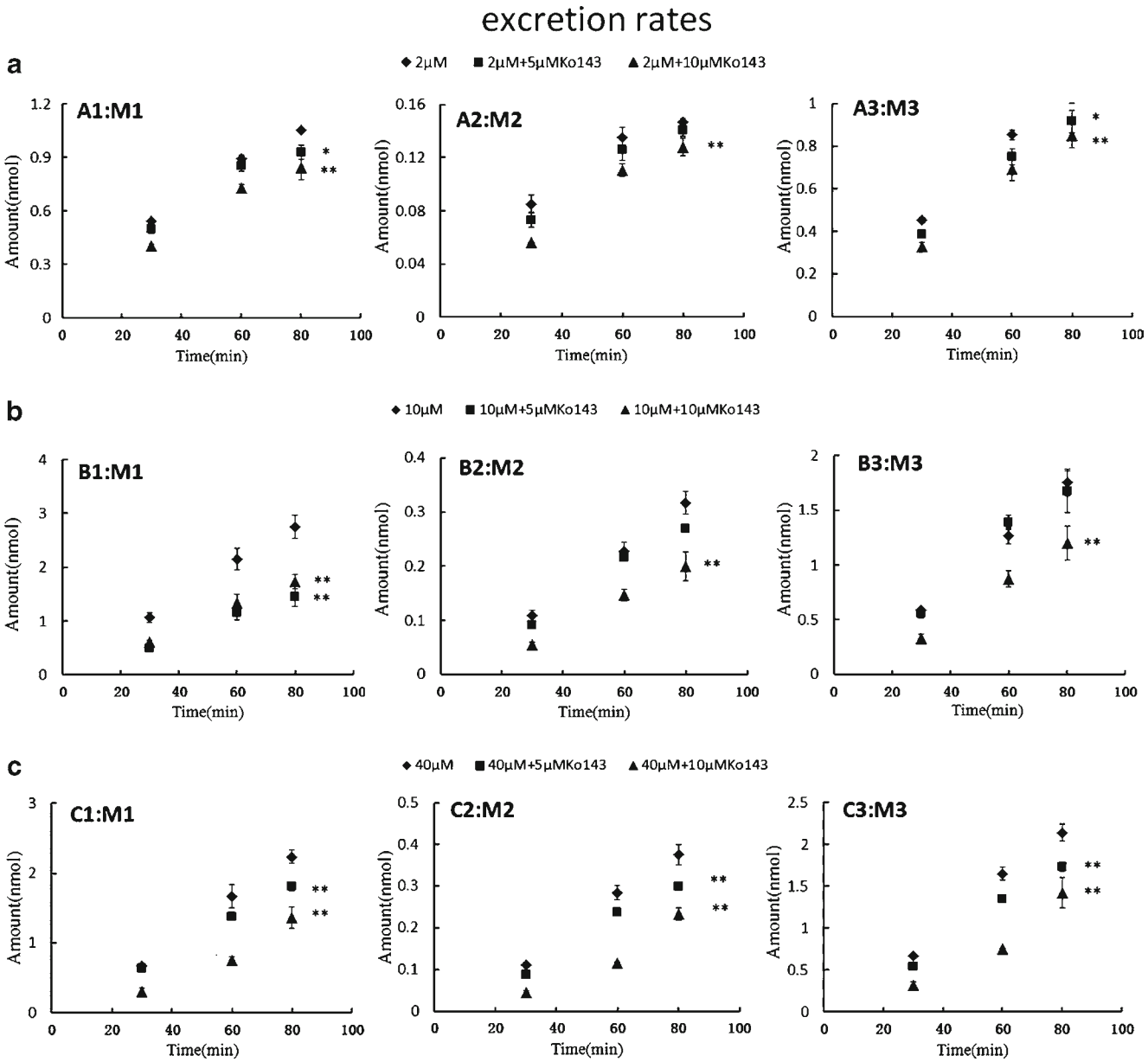

Fig. 6 Effect of the BCRP-specific inhibitor Ko143 on the excretion rate of monoglucuronide (M1-M3). Different concentrations of loading solution (2, 10, and 40 μM) (**a**–**c**), respectively. Engineered HeLa cells stably overexpressing UGT1A9 grown on six-well plates (2×10^5 cells/well) were treated with 2, 10, and 40 μM of luteolin in the absence or presence of Ko143 at 5 or 10 μM. The samples were taken at 30, 60, and 80 min. Each data point is the average of three determinations, with the error bar representing the S.D. ($n=3$). *, $p<0.05$; **, $p<0.01$. *CTR* control.

normalized Vmax values of UGT1A9s from the two sources above were 8.88±0.33 pmol/min/mg *vs.* 13.32±0.32 pmol/min/mg for M1, 1.33±0.049 pmol/min/mg *vs.* 1.43±0.015 pmol/min/mg for M2, and 5.11±0.15 pmol/min/mg *vs.* 6.00±0.12 pmol/min/mg for M3 (Fig. 3, Table II), suggesting that UGT1A9 protein level was the main determining factor of total UGT1A9 activity.

In conclusion, this work delineated the interplay between UGT1A9 and efflux transporter BCRP in luteolin metabolism and disposition at the kinetic level, which could help us understand and predict BCRP-mediated glucuronide clearance *in vivo*. In addition, a novel luteolin diglucuronide, namely 3′- and 4′-conjugated luteolin diglucuronide was detected for the first time. Our data indicated that luteolin diglucuronide was formed from monoglucuronides when the later were present at high levels (>0.07 nM) in HeLa1A9 cells and the conversion was catalyzed primarily by UGT1A9. It was speculated that the production of diglucuronide may be an important compensatory pathway of luteolin disposition *in vivo*.

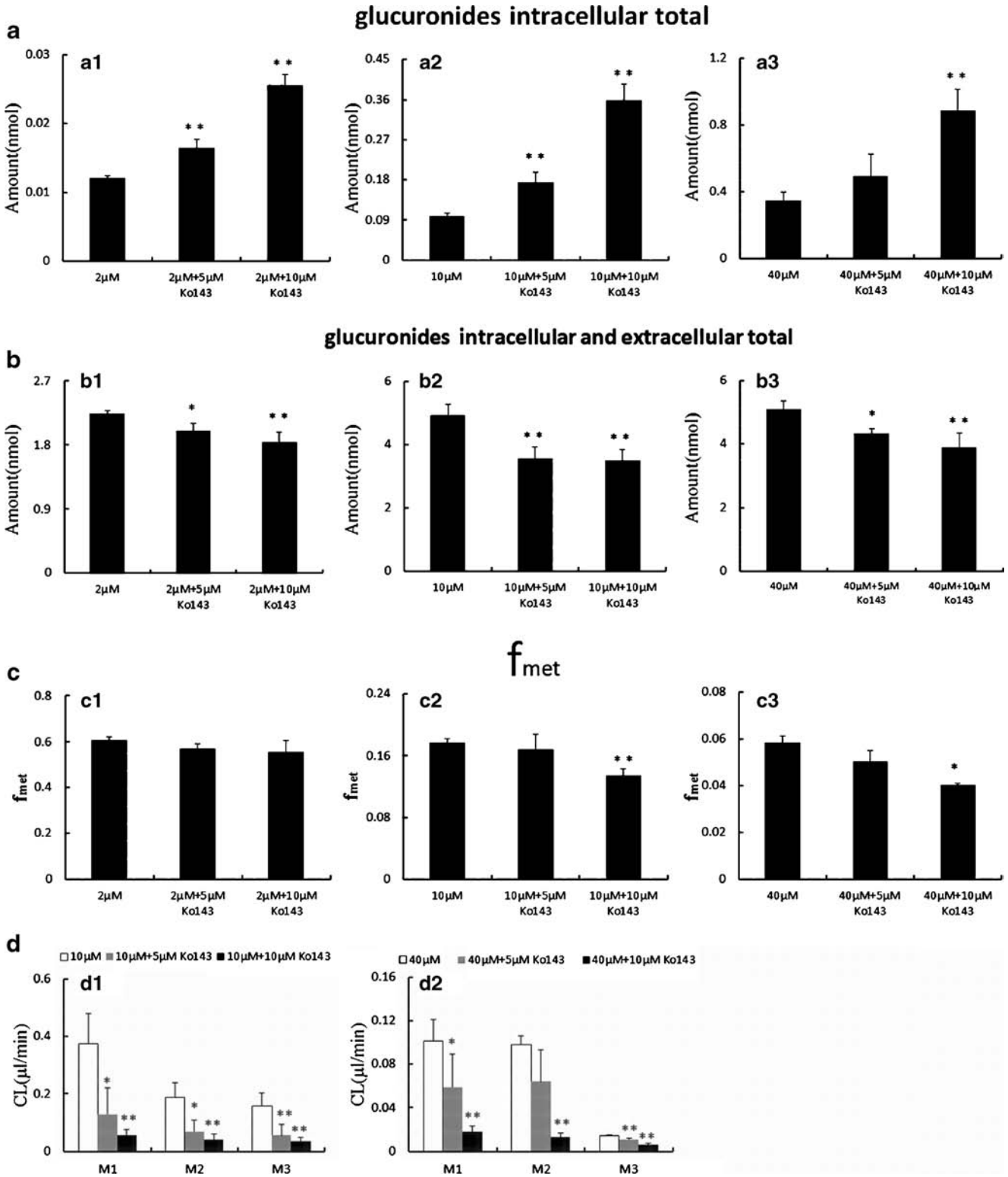

Fig. 7 Effect of the BCRP-specific inhibitor Ko143 on the total intracellular amount of the three monoglucuronides (**a**), total amount of intracellular and extracellular monoglucuronides (**b**), f_{met} (**c**), and CL (**d**). Different concentrations of loading solution (2, 10, and 40 μM) of f_{met} (**a**), similar to (**b**) and (**c**). The amount of metabolites was determined at the end of the experiment described in Fig. 4. The CL values of luteolin (10 and 40 μM) with or without Ko143 (**d**). Each column represents the average of three determinations, with the error bar representing the S.D. of the mean. *, $p < 0.05$; **, $p < 0.01$.

ACKNOWLEDGMENTS AND DISCLOSURES

Lan Tang, Ye Li, Southern Medical University and Guangzhou University of Chinese Medicine contributed equally to this paper. This work was in part supported by the Programs for Fundamental Research and Development (973 program) [2009CB522800], Project of National Natural Science Foundation of China [81001690], the key Project of National Natural Science Foundation of China [U1203204], the Key International Joint Research Project of National Natural Science Foundation of China (81120108025), as well as the Program for Pearl River New Stars of Science and Technology in Guangzhou (2012J2200048). WJ and MH were supported by The National Institutes of Health grant NIH GM070737. The authors report no declaration of interest.

REFERENCES

1. Lopez-Lazaro M. Distribution and biological activities of the flavonoid luteolin. Mini Rev Med Chem. 2009;9:31–59.
2. Lin Y, Shi R, Wang X, Shen HM. Luteolin, a flavonoid with potential for cancer prevention and therapy. Curr Cancer Drug Targets. 2008;8:634–46.
3. Seelinger G, Merfort I, Schempp CM. Anti-oxidant, anti-inflammatory and anti-allergic activities of luteolin. Planta Med. 2008;74:1667–77.
4. Boersma MG, van der Woude H, Bogaards J, Boeren S, Vervoort J, Cnubben NH. Regioselectivity of phase II metabolism of luteolin and quercetin by UDP-glucuronosyl transferases. Chem Res Toxicol. 2002;15:662–70.
5. Shimoi K, Saka N, Kaji K, Nozawa R, Kinae N. Metabolic fate of luteolin and its functional activity at focal site. Biofactors. 2000;12:181–6.
6. Zhou P, Li LP, Luo SQ, Jiang HD, Zeng S. Intestinal absorption of luteolin from peanut hull extract is more efficient than that from individual pure luteolin. J Agric Food Chem. 2008;56:296–300.
7. Shimoi K, Okada H, Furugori M, Goda T, Takase S, Suzuki M, *et al*. Intestinal absorption of luteolin and luteolin 7-O-beta-glucoside in rats and humans. FEBS Lett. 1998;438:220–4.
8. Chen ZS, Robey RW, Belinsky MG, Shchaveleva I, Ren XQ, Sugimoto Y, *et al*. Transport of methotrexate, methotrexate polyglutamates, and 17beta-estradiol 17-(beta-D-glucuronide) by ABCG2: effects of acquired mutations at R482 on methotrexate transport. Cancer Res. 2003;63:4048–54.
9. Xu H, Kulkarni KH, Singh R, Yang Z, Wang SW, Tam VH, *et al*. Disposition of naringenin via glucuronidation pathway is affected by compensating efflux transporters of hydrophilic glucuronides. Mol Pharm. 2009;6:1703–15.
10. Liu ZQ, Jiang ZH, Liu L, Hu M. Mechanisms responsible for poor oral bioavailability of paeoniflorin: role of intestinal disposition and interactions with sinomenine. Pharm Res. 2006;23:2768–80.
11. Zhou GY, Wu D, Snyder B, Ptak RG, Kaur H, Gochin M. Development of indole compounds as small molecule fusion inhibitors targeting HIV-1 glycoprotein-41. J Med Chem. 2011;54:7220–31.
12. Jiang W, Xu B, Wu B, Yu R, Hu M. UDP-glucuronosyltransferase (UGT) 1A9-overexpressing HeLa cells is an appropriate tool to delineate the kinetic interplay between breast cancer resistance protein (BRCP) and UGT and to rapidly identify the glucuronide substrates of BCRP. Drug Metab Dispos. 2012;40:336–45.
13. Wu B, Jiang W, Yin T, Gao S, Hu M. A new strategy to rapidly evaluate kinetics of glucuronide efflux by breast cancer resistance protein (BCRP/ABCG2). Pharm Res. 2012;29:3199–208.
14. Hosoda K, Furuta T, Yokokawa A, Ishii K. Identification and quantification of daidzein-7-glucuronide-4′-sulfate, genistein-7-glucuronide-4′-sulfate and genistein-4′,7-diglucuronide as major metabolites in human plasma after administration of kinako. Anal Bioanal Chem. 2010;397:1563–72.
15. Crawford JM, Ransil BJ, Narciso JP, Gollan JL. Hepatic microsomal bilirubin UDP-glucuronosyltransferase. The kinetics of bilirubin mono- and diglucuronide synthesis. J Biol Chem. 1992;267:16943–50.
16. Chen Z, Kong S, Song F, Li L, Jiang H. Pharmacokinetic study of luteolin, apigenin, chrysoeriol and diosmetin after oral administration of Flos Chrysanthemi extract in rats. Fitoterapia 2012;83(8):1616–22.
17. Tang L, Ye L, Singh R, Wu B, Lv C, Zhao J, *et al*. Use of glucuronidation fingerprinting to describe and predict mono- and dihydroxyflavone metabolism by recombinant UGT isoforms and human intestinal and liver microsomes. Mol Pharm. 2010;7:664–79.
18. Dong RH, Fang ZZ, Zhu LL, Liang SC, Ge GB, Yang L, *et al*. Investigation of UDP-glucuronosyltransferases (UGTs) inhibitory properties of carvacrol. Phytother Res. 2012;26:86–90.
19. Zamek-Gliszczynski MJ, Nezasa K, Tian X, Kalvass JC, Patel NJ, Raub TJ, *et al*. The important role of Bcrp (Abcg2) in the biliary excretion of sulfate and glucuronide metabolites of acetaminophen, 4-methylumbelliferone, and harmol in mice. Mol Pharmacol. 2006;70:2127–33.
20. Wang SW, Chen J, Jia X, Tam VH, Hu M. Disposition of flavonoids via enteric recycling: structural effects and lack of correlations between in vitro and in situ metabolic properties. Drug Metab Dispos. 2006;34:1837–48.
21. Hutzlerand JM, Tracy TS. Atypical kinetic profiles in drug metabolism reactions. Drug Metab Dispos. 2002;30:355–62.
22. Pang KS, Maeng HJ, Fan J. Interplay of transporters and enzymes in drug and metabolite processing. Mol Pharm. 2009;6:1734–55.
23. Yamaguchi H, Yano I, Hashimoto Y, Inui KI. Secretory mechanisms of grepafloxacin and levofloxacin in the human intestinal cell line caco-2. J Pharmacol Exp Ther. 2000;295:360–6.
24. Liu W, Feng Q, Li Y, Ye L, Hu M, Liu Z. Coupling of UDP-glucuronosyltransferases and multidrug resistance-associated proteins is responsible for the intestinal disposition and poor bioavailability of emodin. Toxicol Appl Pharmacol. 2012;265:316–24.
25. Brand W, van der Wel PA, Rein MJ, Barron D, Williamson G, van Bladeren PJ, *et al*. Metabolism and transport of the citrus flavonoid hesperetin in Caco-2 cell monolayers. Drug Metab Dispos. 2008;36:1794–802.
26. Harbourt DE, Fallon JK, Ito S, Baba T, Ritter JK, Glish GL, *et al*. Quantification of human uridine-diphosphate glucuronosyl transferase 1A isoforms in liver, intestine, and kidney using nanobore liquid chromatography-tandem mass spectrometry. Anal Chem. 2012;84:98–105.
27. Bock KW, Raschko FT, Gschaidmeier H, Seidel A, Oesch F, Grove AD, *et al*. Mono- and Diglucuronide formation from benzo[a]pyrene and chrysene diphenols by AHH-1 cell-expressed UDP-glucuronosyltransferase UGT1A7. Biochem Pharmacol. 1999;57:653–6.
28. Udomuksorn W, Elliot DJ, Lewis BC, Mackenzie PI, Yoovathaworn K, Miners JO. Influence of mutations associated with Gilbert and Crigler-Najjar type II syndromes on the glucuronidation kinetics of bilirubin and other UDP-glucuronosyltransferase 1A substrates. Pharmacogenet Genomics. 2007;17:1017–29.
29. Pick A, Muller H, Mayer R, Haenisch B, Pajeva IK, Weigt M, *et al*. Structure-activity relationships of flavonoids as inhibitors of breast cancer resistance protein (BCRP). Bioorg Med Chem. 2011;19:2090–102.
30. Bockand KW, Kohle C. Topological aspects of oligomeric UDP-glucuronosyltransferases in endoplasmic reticulum membranes: advances and open questions. Biochem Pharmacol. 2009;77:1458–65.